Logarithmic discretization and systematic derivation of shell models in two-dimensional turbulence

Ö. D. Gürcan,[1,2,3,4] P. Morel,[3,1,2,4] S. Kobayashi,[1,2] Rameswar Singh,[1,2] S. Xu,[1,3] and P. H. Diamond[5]

[1]*Laboratoire de Physique des Plasmas, Ecole Polytechnique, F-91128 Palaiseau Cedex, France*

[2]*CNRS, UMR7648, Laboratoire de Physique des Plasmas, F-91128, Palaiseau, France*

[3]*Université Paris-Sud, UMR7648, Laboratoire de Physique des Plasmas, F-91128, Palaiseau, France*

[4]*Sorbonne Universités, UPMC Univ Paris 06, UMR7648, Laboratoire de Physique des Plasmas, F-91128, Palaiseau, France*

[5]*CASS and Department of Physics, University of California San Diego, La Jolla, California 92093-0424, USA*

(Received 8 January 2016; revised manuscript received 5 July 2016; published 13 September 2016)

A detailed systematic derivation of a logarithmically discretized model for two-dimensional turbulence is given, starting from the basic fluid equations and proceeding with a particular form of discretization of the wave-number space. We show that it is possible to keep all or a subset of the interactions, either local or disparate scale, and recover various limiting forms of shell models used in plasma and geophysical turbulence studies. The method makes no use of the conservation laws even though it respects the underlying conservation properties of the fluid equations. It gives a family of models ranging from shell models with nonlocal interactions to anisotropic shell models depending on the way the shells are constructed. Numerical integration of the model shows that energy and enstrophy equipartition seem to dominate over the dual cascade, which is a common problem of two-dimensional shell models.

DOI: 10.1103/PhysRevE.94.033106

I. INTRODUCTION

Turbulence is one of the most complex problems in nature. It is an ubiquitous phenomenon involving a multitude of scales and a variety of behaviors, yet, with clear underlying regularities. The self-similar turbulent cascade of conserved quantities such as energy, helicity, enstrophy, etc., in different kinds of physical problems are prime examples of such underlying order. Study of turbulence therefore focuses on simplifying its description using such regularities in order to improve our overall understanding of its important features. The field of turbulence is abound with different approaches to this end, from analytical simplifications to complex modeling efforts.

Numerical simulations provide an important tool for the study of turbulence. Using massive parallelization and innovative numerical schemes, one can simulate a wide range of scales. However, some interesting problems in nature require such a large range of scales between the injection and the dissipation that they may fall out of the reach of modern computing capabilities.

If such a problem can be reduced to a single dimension, by making some reasonable assumptions about the resulting spectral form, or the nature of the turbulence, it can be approached by using a logarithmic grid. This can enhance the available wave-number range considerably. This is commonly done, for example, in the study of weak wave turbulence using wave kinetic equation (e.g., [1] for weak MHD turbulence) since, in that case, one can link the frequency and the wave number using the dispersion relation. It is also employed in closure calculations such as computations with the direct interaction approximation or the eddy damped quasinormal Markovian closure [2–4], differential approximation models [5–7], where isotropy and local interaction assumptions lead to the transformation of the integrodifferential equation in k space, to a simple differential equation. However, extending the concept of logarithmic grid to higher dimensions, and still being able to compute convolution integrals in k space in an effective way is nontrivial [8]. Here, we present one such logarithmically discretized model (LDM), together with its detailed derivation for two-dimensional turbulence [9,10].

It is also notable that in the spirit of simplified models, the process of turbulent cascade is sometimes described using shell models (see, for example, Ref. [11]). Shell models have been proposed and used in various physical contexts from basic fluid turbulence [12] to magnetohydrodynamic turbulence [13], to convective turbulence [14], to drift wave turbulence in plasmas [15], to rotating turbulence [16], to superfluid turbulence in helium II [17], etc. More generally, such reduced models have been important historically, either for numerical reasons or for providing a theoretical insight into the phenomenology of turbulence [18–20]. In particular, they have had great success in obtaining results which were inconceivable from microscopic theory, functional analysis, or direct numerical simulations.

A shell model consists of a set of ordinary differential equations that are nonlinearly coupled to represent the cascade process. In its basic form, it is a differential approximation model with built in logarithmic discretization and arbitrary coefficients multiplying the interaction terms. In fact, one can recover smooth differential approximation models in the continuum limits of these models [21–23]. A shell model usually takes only a subset of the total number of possible interactions into account, but by choice of the interaction coefficients, it respects the conservation laws of the fluid system it represents. Shell models are usually, simply *"written"* using these conservation laws, and not derived through a rigorous procedure starting from the initial equations. Earlier attempts at their derivation involves the establishment of their connection to other classes of reduced models called dyadic models [24,25]. In general, the reduction of a continuous system to only a finite number of modes [26], which are chosen to respect the self-similar structure of the original equations, has been studied for earlier high resolution simulation efforts

[27] and has been extended to pseudospectral formulation [28].

One interesting, maybe puzzling, aspect of shell models is the fact that while they rely on a strong truncation of the original system to only local interactions, they manage to preserve both the spectrum and the intermittent character of the fluctuations [29–31], even though the detailed mechanism is probably different [32]. As a side effect of the derivation of the LDM, here we provide a derivation procedure for the shell model for two-dimensional turbulence. The advantage of the systematic derivation procedure is that it also allows a multitude of models in-between the simple Gledzer Ohkitani Yamada (GOY) model and a direct k-space discretization of the fluid equations to be obtained. It also allows for derivation of such models for more complicated systems consisting of multiple fields (reduced MHD, rotating convection, simplified resistive drift wave turbulence, etc.).

Recent work on turbulence on fractal decimated Fourier space [33,34] shows the role and the importance of equipartition in reduced Fourier space and its connection to cascades. In general, if a binning is used, one that contains equal number of modes per bin gives the same equipartition solution as the original system [28]. Since the LDM uses logarithmic spacing, the equipartition in the LDM, similar to shell models, is expected to be unphysical.

Indeed, numerical integration of the LDM shows that energy and enstrophy equipartition among shells seem to dominate over the dual cascade, at least for the inverse energy cascade range as discussed by Aurell *et al.* [35] for two-dimensional shell models. However, since the derivation allows generalization of the shell model approach, and since two-dimensional shell models are used as elements in multishell models [36] or hierarchical tree models [37], the findings presented in this paper remain useful. Furthermore, new developments on turbulence reduction using helical decomposition may actually make it possible to model inverse cascade using shell models [38] and probably by LDMs as well, without resorting to tree models.

It is also important to note that a system with intrinsic linear instability, such as the barotropic instability in geophysical fluid dynamics (GFD) or drift instabilities in magnetized fusion, can not be overwhelmed by unphysical shell equipartition as easily as a driven Euler system. For instance, repeating the derivation presented below for density and plasma vorticity, assuming finite parallel electron conductivity one can derive a generalization of the shell model for the Hasegawa-Wakatani system described in Ref. [39]. This approach also allows the derivation of an LDM as well as a shell model *for any two-dimensional fluid system regardless of its conservation laws*. This is particularly important since the derivation proposed here can be used in any quasi-two-dimensional fluid problem as a foundation. While such an approach for the two-dimensional Navier-Stokes turbulence discussed below is probably unnecessary with today's computational capabilities, it may be essential for other potential applications.

Consider for instance the equation for the advection of a scalar:

$$\left(\frac{\partial}{\partial t}+\mathbf{v}\cdot\nabla\right)h = F - D, \tag{1}$$

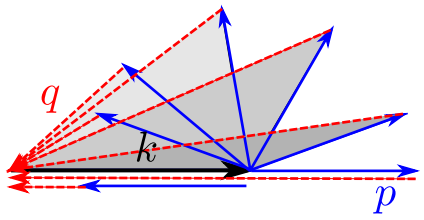

FIG. 1. A cartoon of all possible triads with k and p fixed, such that $k > p$. Note that the minimum and maximum values that q can take are $q_{\min} = k - p$ and $q_{\max} = k + p$. Note that if instead $k < p$, the minimum value would be $q_{\min} = p - k$.

where h can be a passive scalar such as tracer density, or it can be defined in terms of the velocity field as in the case of vorticity for the Euler equation or, more interestingly, potential vorticity for plasma and geophysical turbulence. Here, F and D are some generic forcing and dissipation terms. Considering two-dimensional turbulence, the velocity field can be defined in terms of the stream function $\mathbf{v} = \hat{\mathbf{z}} \times \nabla\Phi$, where $\hat{\mathbf{z}}$ is the direction perpendicular to the plane of motion. Both the $E \times B$ drift velocity and the quasigeostrophic flow velocity can be written this way. Taking the Fourier transform of (1), we obtain

$$\frac{\partial}{\partial t}h(\mathbf{k}) = \frac{1}{(2\pi)^2}\iint (\hat{\mathbf{z}}\times\mathbf{p}\cdot\mathbf{q})\Phi^*(\mathbf{p})h^*(\mathbf{q}) \times \delta(\mathbf{k}+\mathbf{p}+\mathbf{q})d^2\mathbf{p}\,d^2\mathbf{q} + F(\mathbf{k}) - D(\mathbf{k}). \tag{2}$$

The integral is computed over all possible combinations of triangles with sides k, p, and q as shown in Fig. 1. Using polar coordinates $k^2 = k_x^2 + k_y^2$ and $\alpha_k = \tan^{-1}(k_y/k_x)$, we can write this as (see also the Appendix)

$$\begin{aligned}\frac{\partial}{\partial t}h(k,\alpha_k) &= F(k,\alpha_k) - D(k,\alpha_k) + \frac{1}{(2\pi)^2}\iint pq\sin(\alpha_q-\alpha_p) \\ &\times \Phi^*(p,\alpha_p)h^*(q,\alpha_q)\delta(\mathbf{k}+\mathbf{p}+\mathbf{q})pq\,dp\,dq\,d\alpha_p d\alpha_q,\end{aligned} \tag{3}$$

where $\Phi^*(k,\alpha_k) = \Phi(k,\alpha_k+\pi)$ since the original signal $\Phi(x,t)$ is real (similarly for h). The k space can be spanned by writing

$$\begin{aligned}\frac{\partial}{\partial t}h(k,\alpha_k) =& F(k,\alpha_k) - D(k,\alpha_k) \\ &+\frac{1}{(2\pi)^2}\int_0^\infty p\,dp\int_{\alpha_k}^{\alpha_{\max}} d\alpha_p\, pq\sin(\alpha_q-\alpha_p) \\ &\times[\Phi^*(p,\alpha_p)h^*(q,\alpha_q) - \Phi^*(q,\alpha_q)h^*(p,\alpha_p) \\ &+ \Phi^*(q,2\alpha_k-\alpha_q)h^*(p,2\alpha_k-\alpha_p) \\ &- \Phi^*(p,2\alpha_k-\alpha_p)h^*(q,2\alpha_k-\alpha_q)],\end{aligned} \tag{4}$$

where q and α_q are to be interpreted as $q(k,\alpha_k,p,\alpha_p) = |\mathbf{k}+\mathbf{p}|$ and $\alpha_q(k,\alpha_k,p,\alpha_p) = \tan^{-1}[(k\sin\alpha_k + p\sin\alpha_p)/(k\cos\alpha_k + p\cos\alpha_p)]$, respectively. This form includes the contributions from the four triangles, three of which can be obtained by reflections of the first one as shown in Fig. 2.

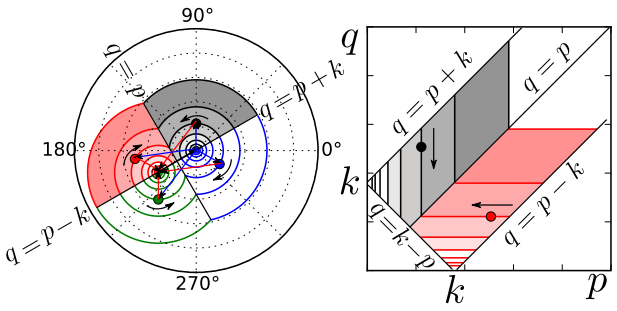

FIG. 2. The integration domain, with logarithmic discretization, is shown on polar coordinates on the left and on a Cartesian representation of p vs q on the right. Here, the vector k is shown in solid black with an angle $\alpha = \pi/6$ to the x axis (just as an example). The vector p is shown in blue and makes an angle $\delta\alpha_{pk} = \alpha_p - \alpha_k$ to the vector k in the first quadrant (gray region in the left figure). Reflecting the triangle across the vector k we obtain another triangle of equal surface area (but a negative sign for the product $\hat{\mathbf{z}} \times \mathbf{p} \cdot \mathbf{q}$), which makes an angle $-\delta\alpha_{pk}$ to the vector k, this corresponds to the fourth quadrant (blue region in the left figure). Similarly, by exchanging the vectors p and q, we obtain the triangle in the third quadrant, which also has the same area. Contributions from these four quadrants give the four terms in Eq. (4).

This allows us to cover the full k space by varying α_p from α_k to an $\alpha_{\max}$, which is either the angle at which $q = p$ (i.e., if $p > k/2$) or $\alpha_k + \pi$ (i.e., if $p > k/2$), and p from 0 to ∞. Note that the contributions from the four quadrants shown in Fig. 2 give the four respective terms in (4). The continuous form given above provides the foundation for the general logarithmic model, which results from the introduction of a logarithmic discretization and a reorganization of the sums in order to exploit the underlying self-similar structure.

The angle between p and q can be computed using the law of cosines as $\cos(\alpha_q - \alpha_p) = (k^2 - p^2 - q^2)/(2pq)$, and therefore

$$\sin(\alpha_q - \alpha_p) = \frac{\pm 1}{2pq}\sqrt{4p^2q^2 - (k^2 - p^2 - q^2)^2} = \frac{\pm 1}{2pq}\sqrt{2q^2(k^2 + p^2) - (k^2 - p^2)^2 - q^4},$$

as needed in (4), and since $\alpha_q - \alpha_p$ for the primary triangle (the upper right one in Fig. 2) is always between 0 and π we can pick the positive root.

Note that for the primary triangle α_p and α_q can be defined in terms of p and q via

$$\alpha_p = \alpha_k + \cos^{-1}\left(\frac{q^2 - k^2 - p^2}{2kp}\right),$$

$$\alpha_q = \alpha_k - \cos^{-1}\left(\frac{p^2 - k^2 - q^2}{2kq}\right).$$

These definitions allow us to consider all possible triads by fixing k and p and varying only q, then changing p and repeating the procedure. Since Eq. (4) is symmetric with respect to an exchange of p and q, when computing the sum, one can consider only the $p < q$ part of the domain.

II. DERIVATION OF THE LOGARITHMICALLY DISCRETIZED MODEL

At this point, in order to derive a logarithmically discretized model (LDM), k space can be divided into shells with $k_n = k_0 g^n$, where $g > 1$ is the logarithmic spacing factor. It is common to use $g = \sqrt{(1+\sqrt{5})/2}$, which allows adjacent k_n's to be perpendicular. In addition, one may also divide each shell into a number of uniform segments using a regular discretization of α_k of the form $\alpha_j = 2\pi j/N_\theta$, where N_θ is the number of poloidal slices, so that $h_n^j \equiv h_{k_n,\alpha_j}$ (see the Appendix for details):

$$\frac{\partial}{\partial t}h_n^j = F_n^j - D_n^j + \left(\sum_{p=0}^{k/2}\sum_{q=k-p}^{k+p} + \sum_{p=k/2}^{\infty}\sum_{q=p}^{k+p}\right)\alpha_{n\ell m} \times \left[\Phi_\ell^{*j+r_{n\ell m}} h_m^{*j-r_{nm\ell}} - h_\ell^{*j+r_{n\ell m}}\Phi_m^{*j-r_{nm\ell}} + h_\ell^{*j-r_{n\ell m}}\Phi_m^{*j+r_{nm\ell}} - \Phi_\ell^{*j-r_{n\ell m}} h_m^{*j+r_{nm\ell}}\right]. \quad (5)$$

Here, $\alpha_{n\ell m}$ is the discretization of $pq\sin(\alpha_q - \alpha_p)$ and

$$r_{n\ell m} = \left\lfloor \frac{N_\theta}{2\pi}\cos^{-1}\left(\frac{q^2 - k^2 - p^2}{2kp}\right)\right\rceil_{n\ell m}, \quad (6)$$

where the brackets $\lfloor \ldots \rceil$ indicate rounding to the closest integer and the sums are computed over discretized values of $p = p_n = k_0 g^n$ and $q = q_n = k_0 g^n$. Recall also that $h_n^{*j} = h_n^{j+N_\theta/2}$ for $j < N_\theta/2$. In fact, the superscripts $j \pm r_{n\ell m}$, etc., in (5) are already to be computed, modulus N_θ, and with the additional symmetry such that $h_n^{j+N_\theta/2} = h_n^{*j}$. Note that for a given $\{n, j\}$ there are four different triads [with $\alpha_j^{'} = 2\pi(j \pm r_{n\ell m})/N_\theta$ and $\alpha_j^{''} = 2\pi(j \pm r_{nm\ell})/N_\theta$] that contribute to the evolution of h_n^j for each value of m and ℓ, over which we compute the sum. As discussed in the Appendix, this reduction is achieved by decimating the continuous Fourier space by considering Dirac delta functions localized at logarithmic grid elements. The result would have an additional weighted sum over j' [where $\alpha_j^{'(j')} = 2\pi(j \pm r_{n\ell m}^{(j')})/N_\theta$ and $\alpha_j^{''(j')} = 2\pi(j \pm r_{nm\ell}^{(j')})/N_\theta$] if we used proper binning (e.g., Ref. [28]) instead of reduction using Dirac delta functions. In fact, the derivation in the Appendix suggests that the interaction coefficients (i.e., $\alpha_{n\ell m}$) should vanish unless the logarithmically discretized wave numbers can form an exact triad. However, the form of the logarithmic grid does not guarantee that discretized values of $\mathbf{p} + \mathbf{q}$ would exactly equal a $\mathbf{k}$ which would also be on the grid. Thus, we use the nearest discrete element to compute the coefficients instead. This allows us to write (6) and introduces discretization error which is expected to reduce with increasing angular resolution. However, as we will see later, this discretization error does not lead to energy nonconservation of the final form even for low angular resolution.

Furthermore, it is important to note that the discretization of $\alpha_{n\ell m}$ and $r_{n\ell m}$ is not unique since k, p, and q can be picked among the possible values with $k \in (k_n, k_{n+1})$, $p \in (k_\ell, k_{\ell+1})$,

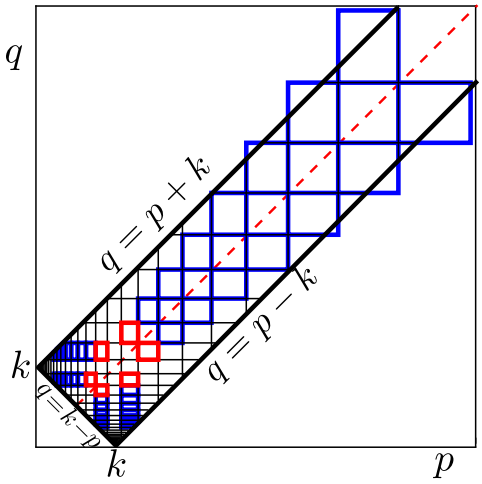

FIG. 3. Discretization of the $p-q$ space due to a discretization of k as $k_n = k_0 g^n$. The red boxes that surround $(p,q) = (k_n,k_n)$ are the shells that are considered in the GOY model, which correspond to setting $m = 0$ in (7). The blue boxes denote the extension as m goes from 0 to N.

and $q \in (k_m,k_{m+1})$. Here, we will pick the basic combination $k = k_n$, $p = k_\ell$, and $q = k_m$, but alternative choices could be invoked in order to maximize the range of possible interactions, which is important if one wants to deal with disparate scale interactions. With these approximations,

$$\alpha_{n\ell m} = k_0^2\sqrt{2g^{2m}(g^{2n}+g^{2\ell})-(g^{2n}-g^{2\ell})^2-g^{4m}}$$

and

$$r_{n\ell m} = \left\lfloor \frac{N_\theta}{2\pi}\cos^{-1}\left(\beta_{n\ell m}\right)\right\rfloor,$$

where $\beta_{n\ell m} = (g^{2m-n-\ell}-g^{n-\ell}-g^{\ell-n})/2$.

At this point, one may reduce the sum by considering only a subset of all possible interactions. Consider, for example, the reduction

$$\begin{aligned}[\ell,m] =& \{[n-2-m',n-1],[n-1-m',n+1],\\ & [n+1+m',n+2+m']\},\end{aligned} \tag{7}$$

which is described in Fig. 3. Considering (5) for the given set above and computing the values of $\alpha_{n\ell m}$ for these combinations (and relabeling m' as m), we obtain

$$\alpha_{n,n-2-m,n-1} = k_n^2 g^{-2m-4}\sqrt{\mu_m(g)},$$
$$\alpha_{nn-1-m,n+1} = k_n^2 g^{-2m-2}\sqrt{\mu_m(g)},$$

and

$$\alpha_{n,n+1+m,n+2+m} = k_n^2\sqrt{\mu_m(g)},$$

where

$$\begin{aligned}\mu_m(g) =& (1+g^{m+1}-g^{m+2})(1-g^{m+1}+g^{m+2})\\ & \times(g^{m+1}+g^{m+2}-1)(1+g^{m+1}+g^{m+2})\end{aligned}$$

and

$$r_m \equiv r_{n,n-2-m,n-1} = \left\lfloor \frac{N_\theta}{2\pi}\cos^{-1}\left[\frac{g^{2m+2}(1-g^2)-1}{2g^{2+m}}\right]\right\rfloor,$$
$$s_m \equiv r_{n,n-1,n-2-m} = \left\lfloor \frac{N_\theta}{2\pi}\cos^{-1}\left[-\frac{g^{2m+2}(1+g^2)-1}{2g^{2m+3}}\right]\right\rfloor,$$
$$\ell_m \equiv r_{n,n-1-m,n+1} = \left\lfloor \frac{N_\theta}{2\pi}\cos^{-1}\left[\frac{g^{2m+2}(g^2-1)-1}{2g^{1+m}}\right]\right\rfloor,$$
$$r_{n,n+1,n-1-m} = s_m,$$
$$r_{n,n+1+m,n+2+m} = \ell_m,$$
$$r_{n,n+2+m,n+1+m} = r_m,$$

which allows us to write (5) as

$$\begin{aligned}\frac{\partial}{\partial t}h_n^j =& F_n^j - D_n^j + \sum_{m=0}^{m_{\max}} k_n^2\sqrt{\mu_m(g)}g^{-1}\\ & \times\{g^{-3-2m}[\Phi^{*j+r_m}_{n-2-m}h^{*j-s_m}_{n-1} - h^{*j+r_m}_{n-2-m}\Phi^{*j-s_m}_{n-1}\\ & + h^{*j-r_m}_{n-2-m}\Phi^{*j+s_m}_{n-1} - \Phi^{*j-r_m}_{n-2-m}h^{*j+s_m}_{n-1}]\\ & + g^{-1-2m}[\Phi^{*j+\ell_m}_{n-1-m}h^{*j-s_m}_{n+1} - h^{*j+\ell_m}_{n-1-m}\Phi^{*j-s_m}_{n+1}\\ & + h^{*j-\ell_m}_{n-1-m}\Phi^{*j+s_m}_{n+1} - \Phi^{*j-\ell_m}_{n-1-m}h^{*j+s_m}_{n+1}]\\ & + g[\Phi^{*j+\ell_m}_{n+1+m}h^{*j-r_m}_{n+2+m} - h^{*j+\ell_m}_{n+1+m}\Phi^{*j-r_m}_{n+2+m}\\ & + h^{*j-\ell_m}_{n+1+m}\Phi^{*j+r_m}_{n+2+m} - \Phi^{*j-\ell_m}_{n+1+m}h^{*j+r_m}_{n+2+m}]\},\end{aligned} \tag{8}$$

where $m_{\max}$ is the largest integer m for which μ_m is positive.

Equation (8) is the general, nonlocal, anisotropic "shell model" and is the final result of this paper. As a matter of fact, (8) is in-between a full logarithmic discretization of the initial fluid system as in (5) and a shell model since it makes no assumption about isotropy and it contains meaningful phase information, unlike a shell model, but it selects only a subset of all possible interactions, even though that subset includes both local and nonlocal interactions. This model can be reduced to various limiting forms to obtain more standard shell models and their generalizations.

A. Conservation laws

The original system as written in (1) conserves only $H = \int h^2 dS$. The discretization above [i.e., Eq. (8)] conserves

$$H = \sum_{n,j}|h_n|^2.$$

This can be shown by multiplying (8) by $h_n^{*j} = h_n^{j+N_\theta/2}$ and summing over j and n:

$$\frac{d}{dt}H = \sum_{n,j}h_n^{*j}\frac{\partial}{\partial t}h_n^j = \mathcal{P}-\mathcal{D}+\overbrace{\sum_{n,j}T_n^j}^{0}. \tag{9}$$

Here, $\mathcal{P} = \sum_{j,n}h_n^{*j}F_n^j$ is the total production and $\mathcal{D} = \sum_{j,n}h_n^{*j}D_n^j$ is the total dissipation of H due to injection and dissipation of h. Conservation of H means that the total transfer due to the nonlinear term vanishes: i.e., $\sum_{n,j}T_n^j = 0$. This can be seen by considering the triads $\{n-2-m,n-1,n\}$,

$\{n-1-m,n,n+1\}$, $\{n,n+1+m,n+2+m\}$, numbering the nonlinear terms in each triad from 1 to 4 [in the order they appear in Eq. (8)], and by letting $n'=n-1$ in the first triad and $n'=n+1+m$ in the last one, in order to write all the triads in the form of the second one, and finally using $r_m=-s_m-\ell_m$ (modulus N_θ). First of all, since $k_n^2 g^{-1-2m}=k_{n+1}^2 g^{-3-2m}=k_{n-1-m}^2 g$, the coefficients of the considered elements of the sum from each triad are the same. It is also easy to see that, when written in this way, the first and the last terms of the first triad are canceled by the last and the first terms of the second triad, the second and the third terms of the first triad are canceled by the first and the last terms of the third triad, and finally the second and the third terms of the second triad are canceled by the third and the second terms of the last triad, giving $\sum_{n,j} T_n^j=0$ already.

Similarly, multiplying (8) by Φ_n^{j*} and summing over j and n, we find that

$$\sum_{j,n}\Phi_n^{j*}\frac{\partial}{\partial t}h_n^j=\mathcal{P}_\phi-\mathcal{D}_\phi+\overbrace{\sum_{n,j}T_{\phi,n}^j}^{0}, \tag{10}$$

where $\mathcal{P}=\sum_{j,n}\Phi_n^{*j}F_n^j$, $\mathcal{D}=\sum_{j,n}\Phi_n^{*j}D_n^j$, and $\sum_{n,j}T_{\phi,n}^j=0$. Same tricks can be used as in the demonstration of the conservation of H, but different terms cancel this time (i.e., the first and the last terms of the first triad are canceled by the second and third terms of the third triad, the second and the third terms of the first triad are canceled by the third and the second terms of the second triad, and the first and the last terms of the second triad are canceled by the last and the first terms of the last triad). This turns into an actual conservation law when one defines h_n^j in terms of Φ_n^j either explicitly or using an evolution equation for Φ_n.

For example, $h_n^j=-k_n^2\Phi_n^j$ turns (9) and (10) into conservation of enstrophy and energy, respectively. Similarly, $h_n^j=(1+k_n^2)\Phi_n^j$ can be used (as potential vorticity) to transform (9) and (10) into conservation of potential enstrophy and energy, etc.

III. REDUCTION TO SIMPLER MODELS

A. Generalized GOY model

It is tempting to start from (8), and make some of the usual assumptions of shell models (such as setting $m_{\max}=0$, and assuming isotropy) to arrive at a shell model. However, it is important to note that if one assumes isotropy of the variables h_n^j and Φ_n^j, the nonlinear term in (8) vanishes. This may seem confusing, but it underlines the important difference between shell models and actual discretizations of fluid systems, namely, the loss of phase information in shell models.

In other words, since the shell model has no information about the phases, we have complete freedom in choosing the $N_\theta\times N$ phases that are defined by $h_n^j=e^{i\theta_n^j}h_n$ and $\Phi_n^j=e^{i\theta_n^j}\Phi_n$. And a particular choice leads to a particular shell model. For instance, if we choose

$$\begin{aligned}\theta_{n-2-m}^{j+r_m}+\theta_{n-1}^{j-s_m}+\theta_n^j&=\theta_{n-1-m}^{j-\ell_m}+\theta_{n+1}^{j+s_m}+\theta_n^j\\&=\theta_{n+1+m}^{j+\ell_m}+\theta_{n+2+m}^{j-r_m}+\theta_n^j=0\end{aligned} \tag{11}$$

for large enough N_θ, this involves $N_\theta[3+2(m_{\max}+1)]$ equations for $N_\theta[5+2(m_{\max}+1)]$ unknowns, and therefore has many possible solutions. This means that all the phases θ_n^j can be obtained in terms of a set of $2N_\theta$ fixed reference phases, such as θ_n^j and $\theta_{n-2-m_{\max}}^j$ or $\theta_{n-2-m_{\max}}^j$ and $\theta_{n+2+m_{\max}}^j$ for example. Assuming that the reference phases are random, averaging over these random phases, we obtain the following generalized shell model:

$$\begin{aligned}\frac{\partial}{\partial t}h_n=&F_n-D_n+\sum_{m=0}^{m_{max}}k_n^2\sqrt{\mu_m(g)}g^{-1}\\&\times\{g^{-3-2m}(\Phi_{n-2-m}^*h_{n-1}^*-h_{n-2-m}^*\Phi_{n-1}^*)\\&-g^{-1-2m}(\Phi_{n-1-m}^*h_{n+1}^*-h_{n-1-m}^*\Phi_{n+1}^*)\\&+g(\Phi_{n+1+m}^*h_{n+2+m}^*-h_{n+1+m}^*\Phi_{n+2+m}^*)\}.\end{aligned}$$

Here, we assumed a slow phase for the complex amplitudes and used the "standard" choice for the phase relations, which results in the conjugation choice consistent with the GOY model. This choice is actually arbitrary in shell models.

Taking h as the vorticity (i.e., $h_n=-k_n^2\Phi_n$), we obtain

$$\begin{aligned}\partial_t\Phi_n=&F_n-D_n+\sum_{m=0}^{m_{\max}}k_n^2\sqrt{\mu_m(g)}g^{-1}\\&\times[(g^2-g^{-2m})g^{-7-2m}\Phi_{n-1}^*\Phi_{n-2-m}^*\\&-(g^4-g^{-2m})g^{-3-2m}\Phi_{n+1}^*\Phi_{n-1-m}^*\\&+(g^2-1)g^{2m+3}\Phi_{n+2+m}^*\Phi_{n+1+m}^*],\end{aligned} \tag{12}$$

which can be seen as a particular generalization of the GOY model for the two-dimensional Navier-Stokes equation, and has the same exact solution

$$\Phi_n\propto\left\{k_n^{-2},k_n^{-4/3}\right\}$$

corresponding to the Kraichnan-Kolmogorov spectra of two-dimensional (2D) turbulence. The generalization in (12) is effectively the same model as that discussed, and extended to the MHD case by Plunian [40] apart from the fact that the extent of the sum (i.e., $m_{\max}$) and the nonlinear interaction coefficients can be computed explicitly here. It is interesting to observe that the extended interactions of this model (in contrast to the GOY model) can be obtained systematically by our approach.

B. Anisotropic 2D shell model

Considering $g>\sqrt{(1+\sqrt{5})/2}$, and $N_\theta=8$, and $m_{\max}=0$ in (8), we get $r_m=3$, $s_m=3$, and $\ell_m=2$. Choosing the phases as in (11) and proceeding as in the previous section leads to elimination of the phase information. Assuming reflection symmetry along x and y axes allows reducing the number of variables to $n_\alpha=N_\theta/4+1$, and therefore defining $h^{(x)}$ as the slice $[-\pi/8,\pi/8]$, $h^{(0)}$ as $[\pi/8,3\pi/8]$, and $h^{(y)}$ as $[3\pi/8,5\pi/8]$ and their reflections. In terms of these, the shell

model can be written as follows:

$$\partial_t h_n^{(x)} = k_n^2\sqrt{\mu(g)}g^{-1}\big[g^{-3}\big(\Phi_{n-1}^{*(0)}h_{n-2}^{*(0)} - \Phi_{n-2}^{*(0)}h_{n-1}^{*(0)}\big) - g^{-1}\big(\Phi_{n+1}^{*(0)}h_{n-1}^{*(y)} - \Phi_{n-1}^{*(y)}h_{n+1}^{*(0)}\big) + g\big(\Phi_{n+2}^{*(0)}h_{n+1}^{*(y)} - \Phi_{n+1}^{*(y)}h_{n+2}^{*(0)}\big)\big], \quad (13a)$$

$$\partial_t h_n^{(y)} = k_n^2\sqrt{\mu(g)}g^{-1}\big[g^{-3}\big(\Phi_{n-1}^{*(0)}h_{n-2}^{*(0)} - \Phi_{n-2}^{*(0)}h_{n-1}^{*(0)}\big) - g^{-1}\big(\Phi_{n+1}^{*(0)}h_{n-1}^{*(x)} - \Phi_{n-1}^{*(x)}h_{n+1}^{*(0)}\big) + g\big(\Phi_{n+2}^{*(0)}h_{n+1}^{*(x)} - \Phi_{n+1}^{*(x)}h_{n+2}^{*(0)}\big)\big], \quad (13b)$$

$$\begin{aligned}\partial_t h_n^{(0)} = {}& \tfrac{1}{2}k_n^2\sqrt{\mu(g)}g^{-1}\big\{g^{-3}\big[\Phi_{n-1}^{*(x)}h_{n-2}^{*(y)} - \Phi_{n-2}^{*(y)}h_{n-1}^{*(x)} + \Phi_{n-1}^{*(y)}h_{n-2}^{*(x)} - \Phi_{n-2}^{*(x)}h_{n-1}^{*(y)}\big] - g^{-1}\big[\Phi_{n+1}^{*(x)}h_{n-1}^{*(0)} - \Phi_{n-1}^{*(0)}h_{n+1}^{*(x)} \\ & + \Phi_{n+1}^{*(y)}h_{n-1}^{*(0)} - \Phi_{n-1}^{*(0)}h_{n+1}^{*(y)}\big] + g\big[\Phi_{n+2}^{*(x)}h_{n+1}^{*(0)} - \Phi_{n+1}^{*(0)}h_{n+2}^{*(x)} + \Phi_{n+2}^{*(y)}h_{n+1}^{*(0)} - \Phi_{n+1}^{*(0)}h_{n+2}^{*(y)}\big]\big\} \end{aligned} \quad (13c)$$

letting $h_n = -k_n^2\Phi_n$, we get the shell model described in Ref. [41].

In fact, writing Eq. (8) directly with $N_\theta = 8$ gives a model similar to the one above, but with four equations and meaningful phase information (i.e., the phases of the discrete variables h_n^m's are not arbitrary as in shell models). It seems that this model, which is not much more complicated than the three-equation model above, should be preferable for most applications.

C. GOY model

Setting $m_{\max} = 0$ in (12) or assuming isotropy in (13a)–(13c), we obtain

$$\begin{aligned}\partial_t \Phi_n = {}& k_n^2\sqrt{\mu(g)}g^{-1}(1-g^2)\big[g^{-7}\Phi_{n-2}^*\Phi_{n-1}^* \\ & - g^{-3}(1+g^2)\Phi_{n-1}^*\Phi_{n+1}^* + g^3\Phi_{n+1}^*\Phi_{n+2}^*\big],\end{aligned}$$

which is the standard 2D version of the GOY model.

D. Disparate scale interactions

The model in (12) can in principle include both local and nonlocal interactions. However, $m_{\max}$ as defined during the derivation of (8) is the largest possible value of m that gives $\mu_m(g) > 0$. One weakness of this approach is its inability to handle truly disparate scale interactions, due to a loss of resolution as n increases. This is seen in Fig. 3, at the smallest scales (largest k) that are visible in the domain. As the centers of the box fall outside the band, their contributions would be excluded. This becomes clear if one derives a disparate scale interaction shell model directly from (8), by taking h_0 (and Φ_0) to represent a dominant large scale mode, and assuming that the energy in k_0 is sufficiently large such that interaction with k_0 for any scale is more important than the interaction with k_1, k_2, etc. This gives

$$\partial_t h_0 = \sum_m k_0^2\sqrt{\mu_m(g)}[(\Phi_{2+m}^*h_{1+m}^* - h_{2+m}^*\Phi_{1+m}^*)], \quad (14)$$

$$\begin{aligned}\partial_t h_n = {}& k_0^2[\sqrt{\mu_{(n-2)}(g)}(\Phi_{n-1}^*h_0^* - h_{n-1}^*\Phi_0^*) \\ & - \sqrt{\mu_{(n-1)}(g)}(\Phi_{n+1}^*h_0^* - h_{n+1}^*\Phi_0^*)] + C_{\rm loc}, \end{aligned} \quad (15)$$

where $C_{\rm loc}$ denote local interactions. The model is somewhat reminiscent of the one discussed in Ref. [22], and assuming h is potential vorticity, it conserves potential enstrophy between disparate scale interactions. However, it is flawed in that it excludes interactions between h_0 and small enough scales for which μ_m becomes negative. One way to fix this would be to define μ_m using a point within the triangular region that remains within the interaction domain (see Fig. 4). Taking $q^2 \approx p^2$, for the equation for the large scale mode (i.e., $\overline{k}$), and $k^2 \approx p^2$ for the equation for small scale mode when computing the angle gives

$$\partial_t \overline{h}_q = \frac{1}{2}\sum_{m=0}^{N}\sqrt{4k_m^2\overline{q}^2 - \overline{q}^4}(\Phi_{m+1}^*h_m^* - h_{m+1}^*\Phi_m^*),$$

$$\begin{aligned}\partial_t h_n = {}& \frac{1}{2}\sqrt{4k_{n-1}^2\overline{q}^2 - \overline{q}^4}[\Phi_{n-1}^*\overline{h}_q^* - h_{n-1}^*\overline{\Phi}_q^*] \\ & - \frac{1}{2}\sqrt{4k_n^2\overline{q}^2 - \overline{q}^4}[\Phi_{n-1}^*\overline{h}_q^* - h_{n-1}^*\overline{\Phi}_q^*],\end{aligned}$$

which becomes exactly the system given in Ref. [22]. In the case $\overline{h}_q = q^2\Phi_q$ and $h_n = (1+k_n^2)\Phi_n$, the exact solution becomes $\Phi_n \propto k_n^{-1/2}/(1+k_n^2)$, which gives $|\Phi_k|^2 \propto k^{-3}/(1+k^2)^2$ as discussed in Refs. [22,42,43].

E. Further generalization

Consider (8). It describes a certain type of "nonlocal" interaction with a certain range $m_{\max}$, with the overall interaction coefficient $\alpha_m = \sqrt{\mu_m(g)}g^{-1}$. On the other hand, Eqs. (14) and (15) describe very nonlocal interactions but with a different interaction coefficient since the area of the region describing these nonlocal interactions is smaller as shown in Fig. 4. In a more general sense, the equation can be written symbolically as

$$\frac{\partial}{\partial t}h_n^j = F_n^j - D_n^j + \sum_{w=0}^{N}\sum_{m=0}^{w}k_n^2\alpha_m^w\{\Phi,h\}_{n\pm1,n\pm2,m}^{j\pm r_{n\pm1,n\pm2,m}^w},$$

where $\{\Phi,h\}_{n\pm1,n\pm2,m}^{j\pm r_{n\pm1,n\pm2,m}^w}$ represents the complicated interaction term inside the curly brackets in (8) (with r_m, s_m, and ℓ_m

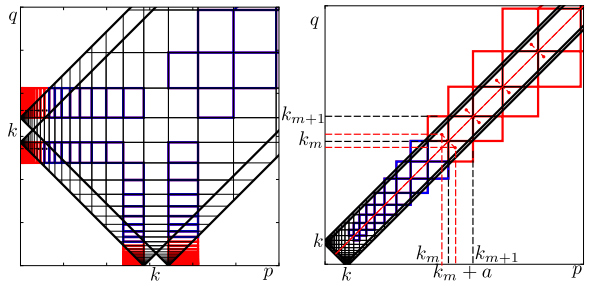

FIG. 4. Disparate scale interactions, and the points at which the coefficient $\sin(\alpha_p - \alpha_q)$, etc., are be computed.

replaced by $r^w_{n\pm1,n\pm2,m}$, etc.). Here, the variable w plays the role of $m_{\max}$ for the second sum. Notice that μ^w_m as well as $r^w_{n\pm1,n\pm2,m}$ depend on the choice of p, q, and k within each box shown in Figs. 3 and 4. Therefore, the sum over w can be interpreted as a sum over subgrid elements. This generalization allows us to consider different interaction coefficients for different interaction ranges. This form corresponds to extending the sum in (8) to N instead of $m_{\max}$, and introducing weights for each term in the sum. If the weight function is simply $\alpha^w_m = \delta_{m_{\max},w}\sqrt{\mu_m}$, we go back to the original system. When the weight function is smoother and more extended, it can represent the ratio of importance of local versus nonlocal versus disparate scale interactions. This formulation corresponds roughly to replacing the original integral in k space by a particular quadrature in a logarithmically discretized space. The coefficients of such a quadrature may be computed uniquely for a given discretization. The details of such a calculation, however, are out of scope of this paper.

IV. NUMERICAL RESULTS

The general logarithmically discretized formulation of the initial fluid system as given in (8) is not very difficult to implement numerically. It is not very easy to run, however, since the result is a stiff set of ordinary differential equations (ODEs) on an exponentially coarse grid. It is essentially similar to a shell model with nonlocal interactions, but with important differences. Namely, that it can handle anisotropy, it has phase information and it includes a range of interactions which are automatically defined via the coarse graining resolution. The phase dynamics of the model depends on the existence of poloidal slices in k space. Therefore, the numerical model must have a minimum poloidal resolution of about $N_\theta = 8$.

In order to implement (8) numerically, we choose $D^j_n = (\nu k_n^4 + \nu_L k_n^{-6})h^j_n$, define $h^j_n = -k_n^2\Phi^j_n$, (i.e., vorticity in two-dimensional Navier-Stokes equation). The forcing is implemented as

$$F^j_n = f_0 e^{[-\frac{1}{2\sigma^2}(j-\frac{N_\theta}{4})^2 + i2\pi\xi]}\left(\delta_{n,n_f} + \delta_{n,n_f+1}\right),$$

which has an amplitude f_0, and is localized on the k_y axis at shells n_f and n_f+1 with a poloidal width σ. Here, ξ is a uniform random number between 0 and 1, and is updated every 10^5 time steps. The model was implemented with a standard, fixed time step, fourth order Runge-Kutta solver using a $c++$ ODE library called odeint [44]. It is important to note that in order for μ_m to be positive, one has to choose $g < (1+\sqrt{5})/2$, which is one of the common values selected for shell models. The isotropized wave-number spectra are presented in Fig. 5. The results for the case (we call it the case 1) $g = 1.56$, $N = 40$, $N_\theta = 32$, $f_0 = 0.01$, $n_f = 20$, $\sigma = 0.4$, $\nu = 10^{-25}$, and $\nu_L = 10^3$, where we can use a time step of $h = 10^{-6}$, are presented in Fig. 6. This choice of g gives $\mu_0 \approx 2.5$ and $m_{\max} = 0$. So, for this choice of parameters the model is anisotropic but actually only has local interactions.

The second case corresponds to the parameters $g = 1.26$, $N = 80$, $N_\theta = 128$, $n_f = 40$ with the rest being the same, where we had to use a time step of $h = 10^{-7}$. This case basically covers the same k range but with a finer resolution. This choice gives $m_{\max} = 4$, and in order to have unique values for r_m, s_m, and ℓ_m (see Table I), we had to increase the poloidal resolution to $N_\theta = 128$. Having sufficient resolution to distinguish these angles seems to be an important aspect for numerical stability. The results for $|\Phi^j_n|^2$ are given in Fig. 7.

TABLE I. Values of r_m, s_m, ℓ_m, and μ_m for the two cases that are considered.

	m	r_m	s_m	ℓ_m	μ_m
Case 1	0	14	15	3	2.50
Case 2	0	45	50	33	6.35
	1	46	53	29	9.85
	2	47	56	25	14.18
	3	49	59	20	17.94
	4	53	61	14	16.07

The spectral energy density $E(k)$ is defined via the basic relation $\int E(k)dk = \sum_n E(k_n)\Delta k_n = \sum_n k_n^2 \frac{2\pi}{N_\theta}\sum_j |\Phi^j_n|^2$, and since in a logarithmic discretization $\Delta k_n \propto k_n$, we can write $E(k_n) = k_n \frac{2\pi}{N_\theta}\sum_j |\Phi^j_n|^2$ as the spectral energy density corresponding to the logarithmically discretized model. The results for the spectral energy density are basically the same for the two cases considered, as can be seen in Fig. 5. While the forward enstrophy cascade range gives $E(k_n) \propto k_n^{-3}$ as expected by Kraichnan-Kolmogorov prediction (even though the "cascade" aspect of this result is also questionable), the inverse energy cascade seems to be not correctly represented by logarithmically discretized model (as is the case with shell models), yielding a "shell-equipartition"

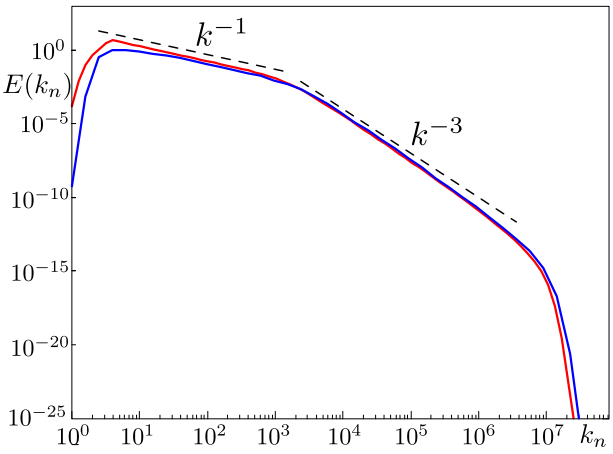

FIG. 5. Energy spectral density $E(k_n) \cong \frac{2\pi}{N_\theta} k_n \sum_j |\Phi^j_n|^2$ as function of k_n for the low resolution local model, i.e., case 1 (blue) and the high resolution nonlocal model, i.e., case 2 (red) discussed in the text. Notice that while the forward enstrophy cascade range gives $E(k) \propto k^{-3}$ as expected by Kraichnan-Kolmogorov spectrum, the inverse energy cascade seems to be not correctly represented by logarithmically discretized model (as with shell models), yielding a "shell-equipartition" result of $E_n = |\Phi_n|^2 k_n^2 = KT$ or $E(k) \propto k^{-1}$.

result of $E_n \propto \sum_j |\Phi_n^j|^2 k_n^2 = KT$ or $E(k_n) \propto k_n^{-1}$. This is already well known in shell models, and it seems that one needs a hierarchical-tree model to get around this issue [35,37].

Note that the fixed time step Runge-Kutte implementation can become numerically unstable for different parameters. It also seems rather difficult to parallelize (an initial attempt to parallelize using OpenMp leads to serious degradation of performance). However, the aim here is not to present a competitive numerical implementation of the model, but rather a proof of principle that demonstrates the feasibility of its numerical implementation.

V. RESULTS AND CONCLUSION

We have developed what we call an LDM, a model which uses logarithmic discretization of the wave-number magnitude similar to shell models, while allowing for anisotropy and phase dynamics via poloidal discretization in k space, for 2D turbulence. Even though the model includes only a reduced subset of all possible interactions, it can account for nonlocal interactions up to a finite range. Such a model can resolve an inertial range of many decades, with a reasonable resolution in the poloidal direction (see Figs. 6 and 7) on a single cpu over a few days.

While in this paper we considered the basic two-dimensional Navier-Stokes equation, variations of such a model (with additional linear terms) can be used for different physical problems such as geophysical turbulence, turbulence in strongly rotating fluids, rotating convection, and turbulence in strongly magnetized plasmas. The derivation outlined in this paper is applicable to those systems simply by replacing h with corresponding fluid quantities, and in particular the potential vorticity.

For the two-dimensional Navier-Stokes equation, the model gives isotropic 2D turbulence spectra, even when it is forced anisotropically. The results seemed to agree well with the Kraichnan-Kolmogorov spectrum of $E(k) \propto k^{-3}$ for the forward enstrophy cascade range, while a shell-equipartition energy spectrum was observed for the large scales in the form of $E(k) \propto k^{-1}$ instead of the inverse energy cascade in accordance with the results of Ref. [35], suggesting that the model is useless as it is, for a direct study of turbulence in 2D fluids. While this is rather discouraging, such models are being used as underlying elements in various more complex models, such as multishell models [36] or hierarchical tree models [37], as well as models that rely mainly on disparate scale interactions [22]. The derivation and the numerical implementation given here are therefore very useful for the development of such tools in cases where anisotropy may be an important feature. Also, a similar approach based on a particular discretization of the Fourier space (i.e., for example a discretization using regular dodecahedron-icosihedron compounds instead of spherical shells [45]) may provide the possibility of extending the current formulation to three dimensions in the future, where the problem of shell equipartition overwhelming the nonlinear cascade should not exist.

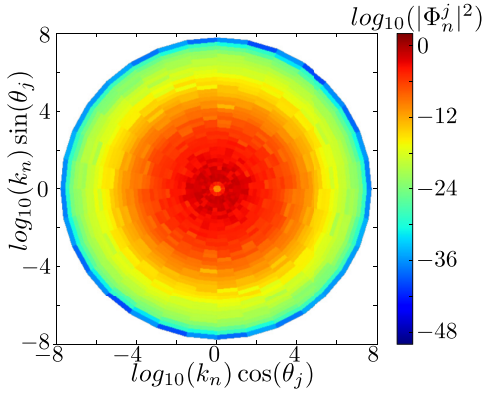

FIG. 6. Turbulence wave-number spectrum in two dimensions for case 1 (i.e., lower resolution, $m_{\max} = 0$).

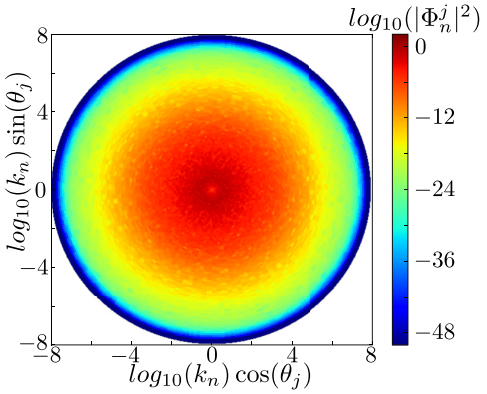

FIG. 7. Turbulence wave-number spectrum in two dimensions for case 2 (i.e., higher resolution with $m_{\max} = 4$).

We have also shown that the LDM can be reduced under some assumptions to various generalized shell models which were previously written based on conservation laws. In particular, it was shown that the nonlocal shell model of Plunian [40], the anisotropic 2D shell model of Gurcan and Grappin [41], and the GOY model and its variations can all be obtained as limiting cases of the LDM discussed in this paper. It was also shown that disparate scale interactions can be added, and a generalization of the LDM can be proposed where another sum can be introduced over interaction ranges, with different weights for each interaction range.

ACKNOWLEDGMENTS

We thank T. S. Hahm, and the other attendants and the organizers of the *Festival de Théorie, Aix en Provence,* for useful discussions. This work is supported by the Direction des Relations Extérieures (DRE) of Ecole Polytechnique and part of it has been done within the LABEX Plas@Par project, and received financial state aid managed by the "Agence Nationale de la Recherche", as part of the "Programme d'Investissements d'Avenir" under the Grant No. ANR-11-IDEX-0004-02. This research was supported in part by the National Science Foundation under Grant No. NSF PHY11-25915.

APPENDIX: LOGARITHMIC DISCRETIZATION AND FOURIER TRANSFORMS

Logarithmic discretization is introduced and used in the main text without mathematical rigor. Here, we attempt to demonstrate that it corresponds to a change of variables of the form $k = k_0 e^{a\kappa}$, where κ becomes the variable of integration in the Fourier transform and establishing the connection to the concept of logarithmic Fourier transform.

Consider the Fourier transform in two dimensions

$$h(\mathbf{k}) = \int h(\mathbf{x}) e^{-i\mathbf{k}\cdot\mathbf{x}} d^2\mathbf{x} = \int h(r,\theta) e^{-ikr\cos(\theta-\alpha)} r\, dr\, d\theta \tag{A1}$$

together with its inverse transform

$$h(r,\theta) = \frac{1}{(2\pi)^2} \int h(k,\alpha) e^{ikr\cos(\alpha-\theta)} k\, dk\, d\alpha\ . \tag{A2}$$

Substituting

$$h(\mathbf{k}) = (2\pi)^2 \sum_{n,m} h_{k_n,\alpha_m} \frac{\delta(k - k_0 g^n)}{k} \delta\left(\alpha - \frac{2\pi}{N_\theta} m\right), \tag{A3}$$

we obtain the logarithmic discretization of $h(\mathbf{k})$. Notice that it is actually based on the transformation $k = k_0 e^{\kappa}$, with a linear discretization in $\kappa \to \kappa_n = n \ln g$ and $\alpha \to \alpha_m = 2\pi m/N_\theta$. Apparently, one can obtain the real field on a logarithmically discretized radial coordinate using a particular inversion algorithm [46].

Note that by taking the continuous Fourier transform of (1),

$$\frac{\partial}{\partial t} h(\mathbf{k},t) = F(\mathbf{k}) - D(\mathbf{k}) + \frac{1}{(2\pi)^2} \int d^2\mathbf{p} \int d^2\mathbf{q} (\hat{\mathbf{z}} \times \mathbf{p} \cdot \mathbf{q}) \times \delta(\mathbf{k} + \mathbf{p} + \mathbf{q}) \Phi^*(\mathbf{p},t) h^*(\mathbf{q},t), \tag{A4}$$

substituting (A3) for h and Φ in (A4) and integrating over one grid element, we obtain the general form

$$\frac{\partial}{\partial t} h_{k_n,\alpha_m} = \sum_{\Delta} pq \sin(\alpha_q - \alpha_p) \Phi_{p,\alpha_p} h_{q,\alpha_q} + F_k - D_k,$$

where the notation Δ for the sum indicates sum over triangles as discussed in the main text. While this has the same form as the discrete sum that results from a bounded system, it already implies a logarithmic grid.

Finally, in order to obtain the real field, we have to compute the inverse Fourier transform. If we substitute (A3) into (A2),

$$h(r,\theta) = \sum_{n,m} h_n^m e^{ik_n r\cos(\alpha_m - \theta)},$$

which we can compute directly using the coefficients h_n^m of the model. This can then be plotted on a regular spatial grid of desired resolution.

[1] S. Galtier, S. V. Nazarenko, A. C. Newell, and A. Pouquet, J. Plasma Phys. **63**, 447 (2000).
[2] C. E. Leith, J. Atmos. Sci. **28**, 145 (1971).
[3] J. C. Bowman, J. Sci. Comput. **11**, 343 (1996).
[4] M. Meldi and P. Sagaut, J. Fluid Mech. **711**, 364 (2012).
[5] D. K. Lilly, J. Atmos. Sci. **46**, 2026 (1989).
[6] V. S. L'vov and S. Nazarenko, JETP Lett. **83**, 541 (2006).
[7] I. Thiagalingam and P. Sagaut, Phys. Fluids **24**, 115109 (2012).
[8] J. C. Bowman, B. A. Shadwick, and P. J. Morrison, Phys. Rev. Lett. **83**, 5491 (1999).
[9] R. H. Kraichnan, Phys. Fluids **10**, 1417 (1967).
[10] R. H. Kraichnan, J. Fluid Mech. **47**, 525 (1971).
[11] L. Biferale, Ann. Rev. Fluid Mech. **35**, 441 (2003).
[12] V. N. Desnianskii and E. A. Novikov, J. Appl. Math. Mech. **38**, 468 (1974).
[13] C. Gloaguen, J. Leorat, A. Pouquet, and R. Grappin, Phys. D (Amsterdam) **17**, 154 (1985).
[14] A. Brandenburg, Phys. Rev. Lett. **69**, 605 (1992).
[15] J. L. Ottinger and D. Carati, Phys. Rev. E **48**, 2955 (1993).
[16] Y. Hattori, R. Rubinstein, and A. Ishizawa, Phys. Rev. E **70**, 046311 (2004).
[17] D. H. Wacks and C. F. Barenghi, Phys. Rev. B **84**, 184505 (2011).
[18] U. Frisch, P.-L. Sulem, and M. Nelkin, J. Fluid Mech. **87**, 719 (1978).
[19] L. Biferale, A. Lambert, R. Lima, and G. Paladin, Phys. D (Amsterdam) **80**, 105 (1995).
[20] V. S. L'vov, E. Podivilov, A. Pomyalov, I. Procaccia, and D. Vandembroucq, Phys. Rev. E **58**, 1811 (1998).
[21] G. Parisi (unpublished).
[22] Ö. D. Gürcan, X. Garbet, P. Hennequin, P. H. Diamond, A. Casati, and G. L. Falchetto, Phys. Rev. Lett. **102**, 255002 (2009).
[23] A. A. Mailybaev, Nonlinearity **28**, 2497 (2015).
[24] N. P. Nets Hawk Katz, Trans. Am. Math. Soc. **357**, 695 (2005).
[25] F. Waleffe, Proc. Am. Math. Soc. **134**, 2913 (2006).
[26] V. Zeitlin, Phys. D (Amsterdam) **49**, 353 (1991).
[27] E. Vázquez-Semadeni and J. Scalo, Phys. Rev. Lett. **68**, 2921 (1992).
[28] J. C. Bowman and M. Roberts, Commun. Nonlin. Sci. Numer. Simul. **17**, 2008 (2012).
[29] K. Ohkitani and M. Yamada, Prog. Theor. Phys. **81**, 329 (1989).
[30] M. H. Jensen, G. Paladin, and A. Vulpiani, Phys. Rev. A **43**, 798 (1991).
[31] D. Pisarenko, L. Biferale, D. Courvoisier, U. Frisch, and M. Vergassola, Phys. Fluids A **5**, 2533 (1993).
[32] S. Grossmann, D. Lohse, and A. Reeh, Phys. Rev. Lett. **77**, 5369 (1996).
[33] U. Frisch, A. Pomyalov, I. Procaccia, and S. S. Ray, Phys. Rev. Lett. **108**, 074501 (2012).

[34] A. S. Lanotte, R. Benzi, S. K. Malapaka, F. Toschi, and L. Biferale, Phys. Rev. Lett. **115**, 264502 (2015).
[35] E. Aurell, P. Frick, and V. Shaidurov, Phys. D (Amsterdam) **72**, 95 (1994).
[36] A. Verdini and R. Grappin, Phys. Rev. Lett. **109**, 025004 (2012).
[37] E. Aurell, E. Dormy, and P. Frick, Phys. Rev. E **56**, 1692 (1997).
[38] M. De Pietro, L. Biferale, and A. A. Mailybaev, Phys. Rev. E **92**, 043021 (2015).
[39] K. Ghantous and O. D. Gürcan, Phys. Rev. E **92**, 033107 (2015).
[40] F. Plunian and R. Stepanov, New J. Phys. **9**, 294 (2007).
[41] Ö. D. Gürcan and R. Grappin, Phys. Rev. E **84**, 066308 (2011).
[42] L. Vermare, P. Hennequin, Ö. D. Gürcan *et al.*, Phys. Plasmas **18**, 012306 (2011).
[43] V. Berionni and Ö. D. Gürcan, Phys. Plasmas **18**, 112301 (2011).
[44] K. Ahnert and M. Mulansky, AIP Conf. Proc. **1389**, 1586 (2011).
[45] Ö. D. Gürcan, A discretization of the wave-number space using a self-similar, alternating, dodecahedral/icosahedral basis for the Navier-Stokes equation, arXiv:1603.01503.
[46] G. V. Haines and A. G. Jones, Geophys. J. Int. **92**, 171 (1988).